OXFORD

human reproduction

Human Reproduction, 2025, **40(9),** 1616–1628

https://doi.org/10.1093/humrep/deaf126

Advance Access Publication Date: July 1, 2025

Original Article

Andrology

CCDC89 is required for optimal sperm motility and male fertility in mammals

Moira K. O'Bryan [1,2], Gülizar Saritas[3,4,5], Joseph Nguyen[1], Sofia B. Winge[3,4], Anne E. O'Connor[1], Helen Castillo-Madeen[6], Donald F. Conrad [2,6], Maddison Graffeo[1], Reza Nosrati[7], Jessica E.M. Dunleavy[1], Kristian Almstrup [2,3,4,5], and Brendan J. Houston [1,*]

[1]School of BioSciences and Bio21 Molecular Sciences and Biotechnology Institute, The University of Melbourne, Parkville, Australia
[2]International Male Infertility Genomics Consortium, IMIGC
[3]Department of Growth and Reproduction, Copenhagen University Hospital—Rigshospitalet, Copenhagen, Denmark
[4]International Center for Research and Research Training in Endocrine Disruption of Male Reproduction and Child Health, Copenhagen University Hospital—Rigshospitalet, Copenhagen, Denmark
[5]Department of Cellular and Molecular Medicine, Faculty of Health and Medical Sciences, University of Copenhagen, Copenhagen, Denmark
[6]Oregon National Primate Research Center, Oregon Health and Science University, Beaverton, OR, USA
[7]Department of Mechanical and Aerospace Engineering, Monash University, Clayton, VIC, Australia

*Correspondence address. School of BioSciences and Bio21 Molecular Sciences and Biotechnology Institute, The University of Melbourne, 30 Flemington Road, Parkville 3052, Australia. E-mail: brendan.houston@unimelb.edu.au https://orcid.org/0000-0002-1078-756X

ABSTRACT

STUDY QUESTION: What is the role of coiled-coil domain-containing protein 89 (CCDC89) in mammalian male fertility?

SUMMARY ANSWER: The presence of CCDC89 is required for normal sperm motility and therefore optimal male fertility in mice, while *CCDC89* variants affected spermatogenesis in both mice and humans.

WHAT IS KNOWN ALREADY: Coiled-coiled domain-containing proteins play a variety of roles in biological processes, including cell division, the production of motile sperm, and the regulation of their motility.

STUDY DESIGN, SIZE, DURATION: DNA from infertile men with azoospermia was sequenced to identify genetic variants as per the Genetics of Male Infertility Initiative (GEMINI) study. Genetic variants were identified in *CCDC89* in three men, by whole exome sequencing. A testis biopsy from infertile Patient 1 (*CCDC89* variant c. G903T) was available and used to inspect tissue pathology. *Ccdc89* knockout (*Ccdc89*$^{-/-}$) and *Ccdc89*$^{E297D/E297D}$ mutant mouse models were generated to define the role of CCDC89 in male fertility and the role of the specific *CCDC89* genetic variant, c. G903T, in the pathogenesis of infertility.

PARTICIPANTS/MATERIALS, SETTING, METHODS: CCDC89 RNA expression and protein localization were investigated in a testis biopsy from a control male with normal spermatogenesis. Male fertility of the mutant mouse lines was assessed via breeding, histology, daily sperm production, electron microscopy, computer-assisted and high-speed sperm motility analysis, and *in vitro* fertilization.

MAIN RESULTS AND THE ROLE OF CHANCE: *Ccdc89*$^{-/-}$ male mice were sub-fertile, with impaired progressive sperm motility and curvilinear velocity due to a rigid sperm tail midpiece without any overt structural defects. While *Ccdc89*$^{E297D/E297D}$ males were fertile, their testis weights and germ cell content were reduced, suggesting a potential role of the c. G903T variant, observed in each of the two men, in the pathogenesis of their spermatogenic impairment. We also identified a new genetic variant in *CCDC89* (c.G1024A) in another infertile man, that was in trans with the c. G903T genetic variant.

LARGE SCALE DATA: N/A.

LIMITATIONS, REASONS FOR CAUTION: The identification of additional infertile men with genetic variants in *CCDC89*, and quality clinical data, are required to determine prognostic reliability regarding *CCDC89* variants. There are likely to be species-specific differences in gene function.

WIDER IMPLICATIONS OF THE FINDINGS: Our data highlight a role for CCDC89, in regulating the sperm tail waveform, that is required for optimal sperm fertilization capacity and male fertility. We highlight CCDC89 as a regulator of male fertility in mammals, where variants in *CCDC89* can affect spermatogenesis and may be a risk factor for human male infertility. This study underscores the importance of validating clinical genetic findings.

STUDY FUNDING/COMPETING INTEREST(S): This work was supported by a National Health and Medical Research Council grant (APP1120356), National Institutes of Health grants (R01HD078641 and P50HD096723), the Novo Nordisk Foundation (grant numbers NNF210C0069913 and NNF21C0069969), the Capital Region of Denmark, the Independent Research Fund (grant number: 1030-00381B), and the Svend Andersen Foundation (grant number: 84-A.08), and the Christian and Ottilia Brorsons (No. 12038-1) and Frimodt-Heineke Foundation travel grants for research exchange. The authors have no conflicts of interest.

Received: January 16, 2025. **Revised:** April 23, 2025. **Editorial decision:** June 3, 2025.

Keywords: genetic variants / male infertility / sperm function / sperm motility / spermatogenesis / CCDC89

Introduction

Male infertility is a highly heterogeneous condition affecting at least 7% men worldwide, with a significant genetic component (Krausz and Riera-Escamilla, 2018; Houston *et al.*, 2021a,c). More than 15 000 human genes are expressed in the testis (Djureinovic *et al.*, 2014; Fagerberg *et al.*, 2014), with most conceivably playing important roles in spermatogenesis but many remaining to be validated via genetic studies and in animal models. In particular, the coiled-coil domain-containing (CCDC) family of genes plays diverse biological roles (Burkhard *et al.*, 2001; Utterstrom *et al.*, 2021). Notably, numerous CCDC family members are enriched within the testis and play essential roles in sperm formation and function (Priyanka and Yenugu, 2021). The CCDC protein superfamily contains more than 700 members that are characterized by the possession of two or more alpha helices that combine to form a superhelix (Burkhard *et al.*, 2001; Moutevelis and Woolfson, 2009; Utterstrom *et al.*, 2021). CCDC proteins play broad roles including as cytoskeletal filaments, components of motor proteins, membrane-anchored recognition proteins, and more (Burkhard *et al.*, 2001). Important to male fertility, several CCDC proteins have been shown to play essential roles in the regulation of centrosome function, sperm tail development, and motile ciliary beating (Yang *et al.*, 2011; Pasek *et al.*, 2016; Wang *et al.*, 2018; Tapia Contreras and Hoyer-Fender, 2019; Bazan *et al.*, 2021; Zhang *et al.*, 2022).

As part of the GEMINI study, we previously identified a novel CCDC protein, *CCDC89*, as a candidate human male fertility gene through the detection of a genetic variant (c.G903T; p. E301D) in two infertile men with azoospermia (Nagirnaja *et al.*, 2022). No functional studies have been undertaken to test the molecular role of *CCDC89* in male fertility or other biological processes. *CCDC89* had, however, been identified as a potential cilium gene based on the CilioGenics study wherein RNA sequencing, protein-protein interactions, and comparative genomics have been used to identify common features of ciliary proteins (Pir *et al.*, 2024). *CCDC89* was also found to be highly expressed within diplotene spermatocytes and round spermatids (Salehi *et al.*, 2021), suggesting a potential role in spermiogenesis or sperm function.

In this study, we aimed to define the role of CCDC89 in male fertility using a knockout mouse model (*Ccdc89*$^{-/-}$). We also aimed to validate the pathogenicity of the specific *CCDC89* homozygous genetic variant (c.G903T; p. E301D) identified in two men with azoospermia by mutating the corresponding amino acid in mice and thus generating a *Ccdc89*$^{E297D/E297D}$ mutant mouse line. Here, we show CCDC89 is required for optimal male fertility.

Materials and methods

Ethics statement

Experimental procedures involving mice followed ethics guidelines published by the Australian National Health and Medical Research Council (NHMRC). All animal experiments were approved by the University of Melbourne Animal Ethics Committee (application 20640). Mice were housed at 20°C on a 14-h light cycle, with standard environmental enrichment, with bedding consisting of corn cob combined with paper twirls and a red Perspex house. Mice were housed according to Code of Practice for the Housing and Care of Laboratory Mice, Rats, Guinea Pigs, and Rabbits. A maximum group of five adult animals was housed in a GM500 individually ventilated cage (Tecniplast, Italy). Ethics for human patient recruitment and sequencing were approved as described previously (Nagirnaja *et al.*, 2022). Relevant ethics approvals for the patients described in this study include the protocol numbers 201107177 and 201109261 approved by: the institutional review board of Washington University in St Louis, USA; the research ethics committee of the Capital Region of Copenhagen (Ref. number H-2-2014-103), the Danish Personal Data Protection Agency (Datatilsynet 2012-58-0004, local number 30-1482, I-Suite 03696), and the European Commission Directive for the transfer of personal data (MTA/I-4728.A1); and the Ethics Committee of National Institute of Health Dr Ricardo Jorge, Lisboa, Portugal. Testis tissue showing full spermatogenesis was retrieved from five men referred for infertility investigation at Department of Growth and Reproduction, Copenhagen University Hospital—Rigshospitalet. This work was approved by the research ethics committee with permit no. H-16019636. Written informed consent was obtained from all men.

Variant detection and pathogenicity assessment

Genetic variants in infertile men presenting with azoospermia were detected using whole exome sequencing and variant quality filtering as described previously (Nagirnaja *et al.*, 2022). Variants in Patient 3 (GEMINI-730) were determined to be in trans based on the predicted variant co-occurrence in gnomAD v2.1.1 (https://gnomad.broadinstitute.org/) and the observation of reads on different alleles in the Integrative Genomics Viewer v2.14.1 (Robinson *et al.*, 2011). MetaDome analysis (https://stuart.radboudumc.nl/metadome/, adapted from Wiel *et al.* (2017, 2019)), CADD score (Kircher *et al.*, 2014), and InterVar (Li and Wang, 2017) assessments were used to infer likelihood of the variants to be disease-causing. A CADD score threshold of at least 15 and an InterVar classification of at least 'variant of unknown significance' was used.

In situ hybridization of CCDC89 transcripts and immunolocalization of CCDC89 protein

Testis tissue was fixed overnight in formaldehyde-based fixative (7.4% formaldehyde, 4% acetic acid, 2% methanol, 0.57% sodium phosphate, and 0.11% potassium phosphate, monobasic), then dehydrated and embedded in paraffin. Sections were cut at 4 µm thickness using a microtome and dried onto glass slides.

CCDC89 protein localization was determined using horseradish peroxidase-based immunohistochemistry, as previously described (Nielsen *et al.*, 2019). Following, dewaxing in xylene and ethanol baths, heat-induced antigen retrieval was undertaken in a medical decloaking chamber (Biocare, Concord, CA, USA) in 0.01 M citrate buffer (pH 6) at 110°C for 30 min. Slides were incubated in 1% (v/v) H_2O_2 in methanol for 30 min and then followed 0.5% skim milk in Tris-buffered saline (TBS) for 30 min to block endogenous peroxidase activity and non-specific protein binding. Sections were incubated overnight at 4°C in a humidified chamber with 0.6 µg/ml CCDC89 antibody (HPA040628; Sigma Aldrich, Germany). The CCDC89 antibody concentration was optimized on testis biopsies from men with full spermatogenesis. Slides incubated with TBS were used as negative controls. After further incubation at room temperature for 1 h, sections were washed in TBS and incubated in anti-rabbit ImmPRESS horseradish peroxidase (Vector laboratories, CA, USA) secondary antibody for

30 min. Slides were visualized with ImmPACT AEC peroxidase substrate (Vector Laboratories) before counterstaining with Mayer's haematoxylin, then mounted with Aquatex® mounting medium (Merck KGaA, Germany).

To investigate *CCDC89* RNA expression in male germ cells, RNA single molecule *in situ* hybridization was performed on human and mouse testis sections using the RNAscope® 2.5 HD Detection Reagent-RED kit (Advanced Cell Diagnostics, CA, USA). Sections were cut at 4 μm thickness and mounted onto SuperFrost Plus™ Slides (ThermoFisher Scientific, MS, USA), dewaxed in xylene, and washed in 100% ethanol, and then treated with H_2O_2 for 10 min. Target retrieval was performed for 15 min at 99°C, followed by treatment with protease plus for 15 (mouse probe) or 30 min (human probe) at 40°C. Sections were hybridized with *CCDC89* RNAscope™ probes (No. Hs-1295821-C1 or Mm-1318181-C1) for 2 h at 40°C, followed by a series of signal amplifications. Sections were counterstained with Mayer's haematoxylin and dried before mounting with Vectamount® Permanent Mounting Medium (Vector Laboratories, CA, USA). The negative control probe DapB (a bacterial RNA, No. 310043) was run in parallel with the *CCDC89/Ccdc89* probe and produced the expected results.

Ccdc89 expression analysis

CCDC89 expression values in human tissues were collected from the GTEx RNA-seq dataset (accession number phs000424.vN.pN) on 29 January 2024. *Ccdc89* expression in mouse testis cell types was extracted from a single-cell sequencing library generated by our laboratory (Jung *et al.*, 2019).

Knockout mouse production

To test the requirement of CCDC89 for male fertility, *Ccdc89* knockout mice were generated on the C57BL/6J background through the Melbourne Advanced Genome Editing Centre (Walter and Eliza Hall Institute, Melbourne, Australia) using CRISPR/Cas9 technology. A humanized point mutant model was also generated to test the impact of the p. E301D variant on male fertility, noting that human CCDC89 amino acid E301 is conserved in mice at residue E297. In mice, *Ccdc89* is a single exon gene. To generate the knockout model, this exon of the sole *Ccdc89* transcript (ENSMUST00000061391.9) was deleted using CRISPR guide RNA sequences: GGTGTCCACTC CCAAAGATA and CTAAACCGTTATCGTTAAAG. For the E297D point mutant model, a single guide RNA, CTAAACCGTTATCG TTAAAG, was used to create double-strand breaks within the *Ccdc89* locus and promote homologous recombination to incorporate the injected oligo donor: CTGTCCATGGAGAGAGGCAAGGTGC TTCAGAACAAACAGGCTGAGATCCGCCAGCTTGAGGAGAAG**ctt**GA-**t**ACAGCAGCCATGGCTAAGAAGCATGCGCTGGAACGCTTTGAGCA-AGAGGCAGTGGCCGTT. The **ctt** sequence denotes the modified amino acid (E297D), while the following GA**t** sequence indicates a silent mutation introduced to prevent cleavage by Cas9 protein.

Changes in gene sequence were identified with Sanger sequencing. Founder mice were bred to wild type to generate founder individuals, which were also Sanger sequenced to confirm inheritance of mutant alleles (Supplementary Table S1). Mice heterozygous for the deletion, or for the point mutation, were crossed to generate homozygous individuals and wild-type controls. Genotyping was performed by Transnetyx (Corvoda, USA). A reduction in *Ccdc89* transcript level (primers F—GGTGTTCAGAACAAACAGGC and R—GCGAACTCTCAGGTTGCTATCA), was verified via qPCR on testis cDNA relative to *Ppia* (primers F—GTCTCCTTCGAGCTGTTT and R—ACCCTGGACATGAATCCT).

Fertility analysis

Mutant males (*Ccdc89*$^{-/-}$ and *Ccdc89*$^{E297D/E297D}$) and wild-type male littermates (*Ccdc89*$^{+/+}$) were aged 10–14 weeks (3 months) or 22–24 weeks (6 months) and their fertility was assessed using the pipeline outlined previously (Houston *et al.*, 2021a). These males were the progeny of heterozygous founders. At least five male mice of each genotype were set up to mate with two wild-type females each (6–12 weeks old), with cages set up in the afternoon and then plugs checked early in the morning. Environmental conditions were identical to those used for standard housing. Litter sizes were recorded as the number of pups generated per plug, where zero denotes no pregnancy. We defined sub-fertility as males generating a litter size significantly less than wild type, but not zero (which would indicate infertility). At least 2 days following mating, males were culled and weighed, and one testis and epididymis were dissected, fixed in Bouin's solution for 5 h and processed for histological assessment (Houston *et al.*, 2021a). Testis sections were stained with periodic acid and Schiff's reagents while epididymis sections were stained with haematoxylin and eosin. After inspecting testis histology, round spermatid numbers were counted in circular profile stage VIII seminiferous tubules ($n = 10$ tubules/animal, $n \geq 5$/genotype) (Houston *et al.*, 2022). Germ cell apoptosis was assessed via staining testis sections with cleaved-Caspase 3 (Cat. No. 9664, Cell Signalling, 0.5 μg/ml) and cleaved-Caspase 7 (Cat. No. 9491, Cell Signalling, 0.23 μg/ml) using standard protocols (Dunleavy *et al.*, 2023) and counting the number of positive cells per tubule ($n = 50$/animal, $n = 3$/genotype).

Additional testes and epididymides were snap-frozen on dry ice for calculation of daily sperm production and epididymal sperm counts as described previously (Dunleavy *et al.*, 2021). In brief, testes and epididymides were solubilized in 1 ml of 1 ml of DSP buffer (0.9% NaCl, 0.01% NaN_3, 0.05% Triton X-100) and sperm number was calculated using a Hirschmann-improved Neubauer haemocytometer with a chamber depth of 0.1 mm.

Sperm flagellum analysis

Sperm from males were collected from the cauda epididymis using the backflushing technique, then resuspended in MT6 medium at 37°C for motility assessment via computer-assisted semen analysis (Houston *et al.*, 2021b). A high-resolution analysis of sperm tail waveform was also undertaken, as previously described (Nandagiri *et al.*, 2021). Sperm were backflushed into TYH medium (10 mM HEPES, 5.6 mM glucose, 1 mM $MgSO_4$, 1.2 mM KH_2PO_4, 2 mM $CaCl_2$, 4.8 mM KCl, 135 mM NaCl, 0.5 mM sodium pyruvate, 10 mM sodium L-lactate, 0.3 mg/ml bovine serum albumin). Imaging chambers were generated by placing two strips of clear tape 15 mm apart on a glass slide. A 10-μl of sperm sample was placed in the chamber and covered with a coverslip (Menzel Gläser, thickness 1.5). Sperm were examined on an Olympus AX-70 microscope fitted with a U-DFA 18 mm internal diameter dark-field annulus and a 20× objective (NA = 0.7, UPlanAPO, Olympus, Japan). Videos were taken using an Andor Zyla 5.5 sCMOS camera using the Fiji image-processing package with the Micro-Manager Studio plugin (version 1.4.23) at 250 frames per second. A minimum of 10 individual 4-s videos were taken and analysed per animal, i.e. each assessing a difference sperm ($n \geq 5$ animals/genotype). Videos were contrasted and processed in Fiji (version 2.9.0/1.53t) before being analysed in MATLAB (version R2023b), using a modified version of the MATLAB codes used previously (Nandagiri *et al.*, 2021) to improve spatial and temporal resolution of flagellar beat analysis, by refining our contour extraction and spline-fitting routines and improve 3D flagellar

waveform reconstruction, enabled by combining our improved 2D tracking with thin-lens approximation (Powar *et al.*, 2022; Yazdan Parast *et al.*, 2023). These codes are publicly available from the Monash University Research Repository (https://doi.org/10.26180/14045816). The sperm flagella centreline was extracted in every frame from each video to reconstruct sperm waveform as previously described (Nandagiri *et al.*, 2021). Simplistically, the sperm tail and head were identified and skeletonized in MATLAB, where the tail was smoothed using low-pass filtering to form a curve that represented the centreline. Curvature kymographs were plotted by calculating the tangent angle of the flagella waveform (MATLAB). Sperm flagella amplitude at the maximum inflection point of the midpiece (0–20 μm) and principal piece (21–80 μm) were calculated in MATLAB by determining the average amplitude along each tail section over each beat cycle. Sperm flagella power in the form of 'motor input' and 'dissipation' were calculated as previously described (Nandagiri *et al.*, 2021). Motor input was defined as the power dissipated by the dynein motors from inputs of other structures in the sperm flagellum (Yazdan Parast *et al.*, 2023). Motor dissipation was defined as the energy dissipated by dynein from inputs of other flagella structures. Similarly, internal dissipation was defined as energy dissipation due to friction between flagellum cross-sectional planes. Hydrodynamic dissipation was defined as energy dissipation from flagella into the surrounding liquid. The energy calculation model was established in Nandagiri *et al.* (2021), which is based on well-defined theoretical models and has been since validated for several other applications (Gaikwad *et al.*, 2021; Yazdan Parast *et al.*, 2023). As a measure of sperm tail stiffness, mean beat cycle graphs were categorized into four main groups based on midpiece amplitude: highly flexible (>23 μm deflection in the Y direction), flexible (>14–23 μm), stiff (5–14 μm), and rigid (<5 μm).

Additional sperm were washed in 1× PBS and dried onto SuperFrost slides before being fixed in 4% paraformaldehyde for 10 min. Cells were washed in PBS and stained with Mayer's haematoxylin for 10 min and eosin (Amber Scientific, Australia) for 1 min to allow an assessment of sperm morphology and tail length. Sperm midpiece and full tail length measurements were measured using ImageJ (version 1.52k).

In vitro fertilization

To test the ability of sperm to achieve fertilization *in vitro*, additional sperm were capacitated in G-IVF PLUS solution (Vitrolife, Australia) for 75 min at 37°C in an atmosphere of 5% O_2/6% CO_2. In parallel, following a standard superovulation approach (Hu *et al.*, 2018), cumulus–oocyte complexes were harvested from the ampullae of 3- to 6-week-old B6xCBAF1/J females. Cumulus–oocyte complexes were washed and then placed in G-IVF PLUS medium supplemented with 1 mM reduced L-glutathione (Sigma Aldrich G4251) (Lord *et al.*, 2013; Martin *et al.*, 2019) at 37°C in an atmosphere of 5% O_2 and6% CO_2. Sperm concentration was determined using a haemocytometer, and a total of 5×10^5 sperm added to each fertilization dish for 4 h at 37°C in 5% O_2 and 6% CO_2. Following the fertilization period, potential zygotes were washed four times in G1 PLUS medium (Vitrolife) before being cultured overnight in G1 PLUS under OVOIL, followed by an assessment of 2-cell development rate.

Electron microscopy

To investigate sperm tail ultrastructure, sperm were backflushed from the cauda epididymis into MT6 medium and processed for electron microscopy as outlined previously (Dunleavy *et al.*, 2017). Images were taken on a Talos L120C or a FEI Teneo VolumeScope at the Ian Holmes Imaging Centre (The University of Melbourne). To view mitochondria and fibrous sheath structure via scanning electron microscopy, sperm were isolated from the cauda epididymis and incubated in 100 μl of 1× PBS for 30 min to strip the plasma membrane, then processed as outlined previously (Korneev *et al.*, 2021). Mitochondrial sheath abnormality was assessed as described previously (Houston *et al.*, 2024).

Statistical analysis

Statistical analyses were performed in Prism 10 (GraphPad, San Diego, USA). A two-way ANOVA was undertaken to determine the effects of genotype, age, or an interaction between both factors, on each biological parameter, with a *post hoc* Dunnett's multiple comparison used to compare genotype groups. When comparing two genotypes (e.g. wild type and *Ccdc89*$^{-/-}$) at a single age point, data were assessed via an unpaired student's *t*-test. Apoptosis data were assessed using an R script, using a generalized linear mixed effects regression (glmer) with a Poisson distribution, where the number of cells was fit as a response variable. Genotype and age and their interaction were assigned as fixed effects and animal number as a random effect. High-resolution sperm tail imaging data were assessed using a Student's *t*-test. A *P*-value <0.05 was considered statistically significant.

Results

Missense variants in CCDC89 are associated with azoospermia and human male infertility

We undertook exome sequencing on a cohort of 924 infertile men presenting with azoospermia (i.e. no sperm in their ejaculate), as reported previously, and as part of the GEMINI study to identify novel genetic causes of human male infertility (Nagirnaja *et al.*, 2022). This approach identified two unique non-synonymous missense variants in *CCDC89* in three men with non-obstructive azoospermic (Table 1, Fig. 1A). Patients 1 and 2 presented with identical biallelic missense variants in *CCDC89* (c.G903T) (Nagirnaja *et al.*, 2022). Patient 3, whose findings have not been published previously, presented with compound heterozygous missense variants in *CCDC89*, including the c. G903T variant on one allele, in trans with the second variant (c.G1024A).

Table 1. *CCDC89* variants identified in infertile men.

			Variant		
Patient	**Origin**	**Infertility type**	**Type**	**cDNA**	**Protein**
1. GEMINI 365	Copenhagen, Denmark	Non-obstructive azoospermia, Sertoli cell only	Homozygous missense	c.G903T	p.E301D
2. GEMINI 1059	St. Louis, USA	Non-obstructive azoospermia, no biopsy taken	Homozygous missense	c.G903T	p.E301D
3. GEMINI 730	Porto, Portugal	Non-obstructive azoospermia, no biopsy taken	Compound heterozygous missense	c.G1024A c.G903T	p.D342N p.E301D

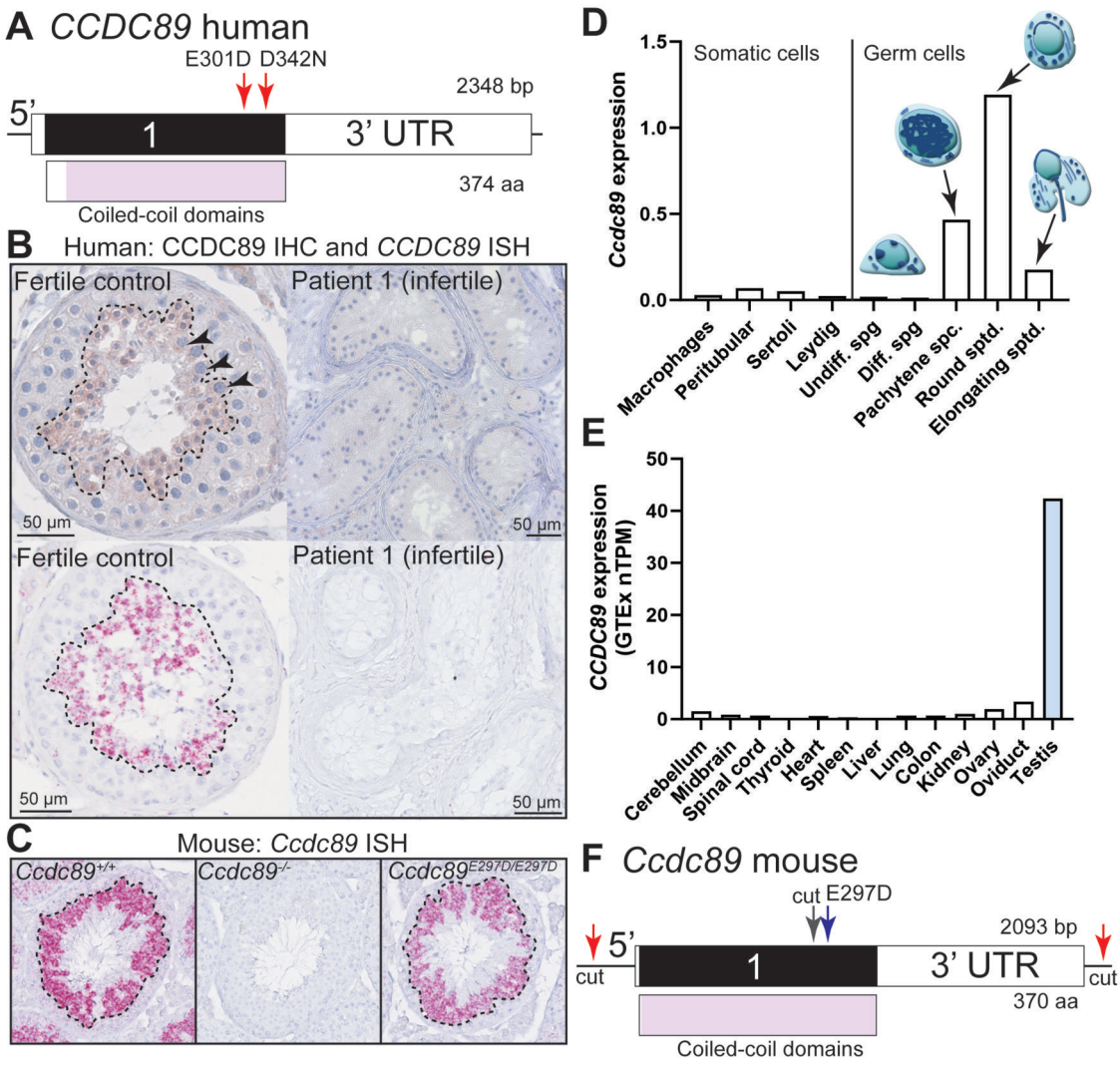

Figure 1. Genetic variants identified in the testis-enriched gene *CCDC89* in infertile men. (**A**) A schematic of the human *CCDC89* gene (bp = base pairs) and protein. The coiled-coil domains are indicated (aa=amino acids). Red arrows indicate genetic variants discovered in three infertile men. (**B**) CCDC89 protein (top) and transcript (bottom) expression in a normal human testis sample and in Patient 1 who carried biallelic p. E301D variants. (**C**) *Ccdc89* mRNA expression in mouse testes in wild type (*Ccdc89*$^{+/+}$) and the two mutant lines investigated in this study. ISH, *in situ* hybridization. (**D**) *Ccdc89* expression (RNA-seq) in testis cells as published in Jung *et al.* (2019). (**E**) *CCDC89* expression in human tissues (RNA-seq) as published in human organ expression data (GTEx). (**F**) A schematic of the mouse *Ccdc89* gene in mice and encoded protein. The coiled-coil domains and cut sites for mutant mouse model production are indicated. Red arrows indicate CRISPR cut sites for the knockout model. The grey arrow indicates the cut site for the donor oligo containing the E297D mutation for the point mutant model.

Both missense variants affected the single exon of the single *CCDC89* transcript reported in humans (ENST00000316398.5). This exon encodes a domain with a continuous region of coiled-coil motifs in the CCDC89 protein (Fig. 1A). The predicted pathogenicity revealed that both affected amino acids were intolerant to change (MetaDome), with tolerance scores of 0.51 (p.E301D) and 0.66 (p.D342N), where lower scores indicating reduced tolerance (Wiel *et al.*, 2019). Similarly, they had CADD scores of 23.5 (p.E301D) and 15.4 (p.D342N), which places the variants among the top 1% and 5% of all deleterious substitutions in the genome. Using the American College of Medical Genetics scoring guidelines (InterVar), the variants were classified as 'variants of unknown significance'. Analysis of CCDC89 protein structure and the potential effects of variants on protein structure were investigated using AlphaFold (Jumper *et al.*, 2021; Varadi *et al.*, 2024) and ColabFold (Mirdita *et al.*, 2022) (Supplementary Fig. S1). Human CCDC89 was predicted to assemble as a predominantly linear protein with most of the protein sequence encoding alpha helices (Supplementary Fig. S1A), which is also the dominant feature of CCDC proteins. The coiled-coil region spanned from amino acid 20-374, with a hinge-like region from residues 52 to 60. Modelling the effects of the E301D variant on CCDC89 structure in ColabFold (Supplementary Fig. S1), we identified a predicted change in the positioning of the 'hinge' region. This region appeared to bend further away from the remainder of the protein. No obvious effects of the D342N variant were identified by protein modelling. pLDDT scores of >80 highlight high confidence in protein structure.

The similarity of CCDC89 protein structure between human and mouse was investigated (Supplementary Fig. S1B). First, using the NCBI basic local alignment sequence tool, we highlighted a 77% protein conservation of CCDC89 from human to mice. The predicted protein structure was largely similar between human and mice. In mice, modelling revealed a modestly shorter coiled-coil region preceding the hinge at the N-terminus, compared to human CCDC89.

Using immunolocalization and RNA *in situ* hybridization (Fig. 1B), we next showed that CCDC89 is expressed at the

transcript and the protein level in round spermatids in human testis biopsies from men with complete spermatogenesis. CCDC89 protein was also observed in spermatocytes (arrowheads). CCDC89 localization and expression were absent from a testicular biopsy taken from infertile patient 1 (GEMINI 365), who exhibited a clear Sertoli cell-only histopathology with no germ cells present. In mouse testes, *Ccdc89* was expressed in round spermatids as determined by *in situ* hybridization (Fig. 1C) and published single-cell RNA sequencing data (Fig. 1D). As reported in human organ expression data (GTEx), *CCDC89* was highly expressed, and enriched, within the human testis (Fig. 1E).

To investigate *Ccdc89* gene function and variant pathogenicity, we generated two mutant mouse models (Fig. 1F). We removed the entire *Ccdc89* coding sequence to generate a knockout mouse model ($Ccdc89^{-/-}$). We also introduced the equivalent p. E297D amino acid using a donor DNA sequence, where mouse p. E297 aligns to human p. E301. This second model ($Ccdc89^{E297D/E297D}$) allowed us to investigate the effect of the missense variant on protein function and thus test the gene–disease relationship.

Ccdc89 is required for optimal male fertility in mice

Males of each genotype were assessed for fertility parameters at 3 and 6 months of age to investigate any compounding effects of age on disease presentation. Deletion of *Ccdc89* was validated by the absence of *Ccdc89* transcripts in the knockout model (Fig. 2A, $P < 0.0001$). Full loss of CCDC89 function rendered male mice sub-fertile (Fig. 2B), with significantly reduced litter sizes (3.7 pups/litter) compared with wild-type littermates (6.86 pups/litter; $P = 0.004$). The loss of *Ccdc89* did not affect body (Fig. 2C), testis (Fig. 2D), or epididymis (Fig. 2H) weight, and spermatogenesis was complete and histologically normal in both wild-type and $Ccdc89^{-/-}$ males (Fig. 2E and F). The loss of CCDC89 did not affect daily sperm production (Fig. 2I), epididymal sperm count (Fig. 2J), or spermatid counts per tubule (Fig. 2K). Similarly, epididymis histology was normal, and sperm were present in all regions (cauda epididymis shown) in both wild-type and $Ccdc89^{-/-}$ males (Fig. 2L and M). $Ccdc89^{-/-}$ females produced litters of normal size (Supplementary Fig. S2).

Examination of sperm from $Ccdc89^{-/-}$ males revealed the cause for sub-fertility was impaired sperm motility (Fig. 3). Computer-assisted sperm analysis revealed that sperm total motility (Fig. 3A; $P = 0.0008$) and progressive motility (Fig. 3B; $P = 0.026$), as well as curvilinear velocity (Fig. 3C; $P < 0.0001$) were reduced in young mice $Ccdc89^{-/-}$ males compared to wild type. These reductions were maintained at 6 months of ages. Sperm morphology was normal in $Ccdc89^{-/-}$ males (Fig. 3D and E; $P = 0.11$), including having a normal sperm total tail and midpiece length (Fig. 3F; $P = 0.09$ and 0.96, respectively). Inspection of the internal sperm tail structures was undertaken using scanning electron microscopy on plasma membrane-stripped sperm from wild-type and $Ccdc89^{-/-}$ males (Fig. 3G and H). This analysis revealed a normal mitochondrial sheath with compacted and intercalated mitochondria in the midpiece, and an intact fibrous sheath spanning the principal piece. Similarly, inspection of the sperm tail core ultrastructure using transmission electron microscopy revealed a normal axoneme structure, containing comparable microtubule doublets and outer dense fibres (Fig. 3I–L). In the midpiece, mitochondria were present and normally arranged, while in the principal piece, the fibrous sheath was present and superficially normal.

Ccdc89 missense variant E297D impairs mouse testis sperm count

No significant change in *Ccdc89* transcript abundance was observed in $Ccdc89^{E297D/E297D}$ males relative to wild type (Fig. 2A, $P = 0.2$). $Ccdc89^{E297D/E297D}$ males (Fig. 2B) and females (Supplementary Fig. S1) produced litters of normal size compared to wild type. No difference in body (Fig. 2C) or epididymis (Fig. 2H) weights were detected relative to wild type. Notably, testis weight from young $Ccdc89^{E297D/E297D}$ males was reduced by 10% compared with both wild-type and $Ccdc89^{-/-}$ males (Fig. 2D, $P < 0.0001$). Testis weights of aged $Ccdc89^{E297D/E297D}$ males were also significantly reduced by 11% compared to $Ccdc89^{-/-}$ males ($P = 0.0003$) but not wild-type males (5% reduction, $P = 0.23$). Similarly, young $Ccdc89^{E297D/E297D}$ males generated 22% fewer sperm than wild type (Fig. 2I; $P = 0.002$). Despite a reduction in testis weight and daily sperm production, spermatogenesis (Fig. 2G) was complete and histologically normal in $Ccdc89^{E297D/E297D}$ males. Epididymal sperm count (Fig. 2J) and epididymis histology (Fig. 2N) were comparable between $Ccdc89^{E297D/E297D}$ and wild-type males (Fig. 2J).

To investigate the origin of reduced sperm production, round spermatid numbers were counted in stage VIII tubules (Fig. 2K). This revealed a reduction in the round spermatid count per tubule in $Ccdc89^{E297D/E297D}$ males compared with wild-type and $Ccdc89^{-/-}$ males at both age points ($P < 0.05$). No differences in the number of apoptotic cells were observed in the testes of $Ccdc89^{-/-}$ males nor $Ccdc89^{E297D/E297D}$ males compared to wild type (Supplementary Fig. S3).

CCDC89 is required for sperm midpiece flexibility and normal sperm tail waveform

To assess the role of CCDC89 in sperm motility more completely, we used a high-speed and resolution waveform analysis on head-tethered sperm (Nandagiri *et al.*, 2021). As sperm from $Ccdc89^{E297D/E297D}$ males exhibited no sperm motility or morphology defects as assessed by computer-assisted semen analysis and histology (Fig. 3A–F), we focused this analysis on sperm from $Ccdc89^{-/-}$ males. While wild-type sperm exhibited a periodic and flexible waveform throughout the entire sperm tail (Video 1), sperm from $Ccdc89^{-/-}$ males were inflexible in the midpiece and exhibited a constrained waveform (Video 2).

To quantify these defects, tail beat frequency, shape cycle, and flagellar curvature were analysed (Figs 4 and 5). Sperm tail beating patterns were analysed by plotting the average flagellar waveform over a beat cycle to produce a representative waveform (Fig. 4A). In wild-type sperm, 29% of sperm midpieces were highly flexible (Fig. 4Ai), 43% were flexible, while 18% were stiff and 10% were rigid (Fig. 4Aii, Supplementary Fig. S4). By contrast, in $Ccdc89^{-/-}$ males, only 5% of sperm midpieces were highly flexible and 15% were flexible (Fig. 4Aiv). Conversely, the proportion of sperm with a stiff or rigid midpiece from $Ccdc89^{-/-}$ males was significantly elevated, at 80% (Fig. 4Av and vi), compared with only 28% of sperm from wild-type male mice (Figs 4Aiii and 5C, $P = 0.006$).

Data extracted from the waveform analysis further allowed construction of the flagella shape cycle, based on the first two dominant modes of flagella shape as a measure of flagella waveform reproducibility (Nandagiri *et al.*, 2021). Sperm from wild-type males produced a circular shape cycle (Fig. 4Bi–iii), indicating a highly reproducible and consistent flagella waveform over multiple beat cycles. In contrast, sperm from $Ccdc89^{-/-}$ males produced an irregular shape cycle (Fig. 4Bv–viii). In sperm with flexible (Fig. 4Bv and vi) and stiff (Fig. 4Bvii) midpieces, the

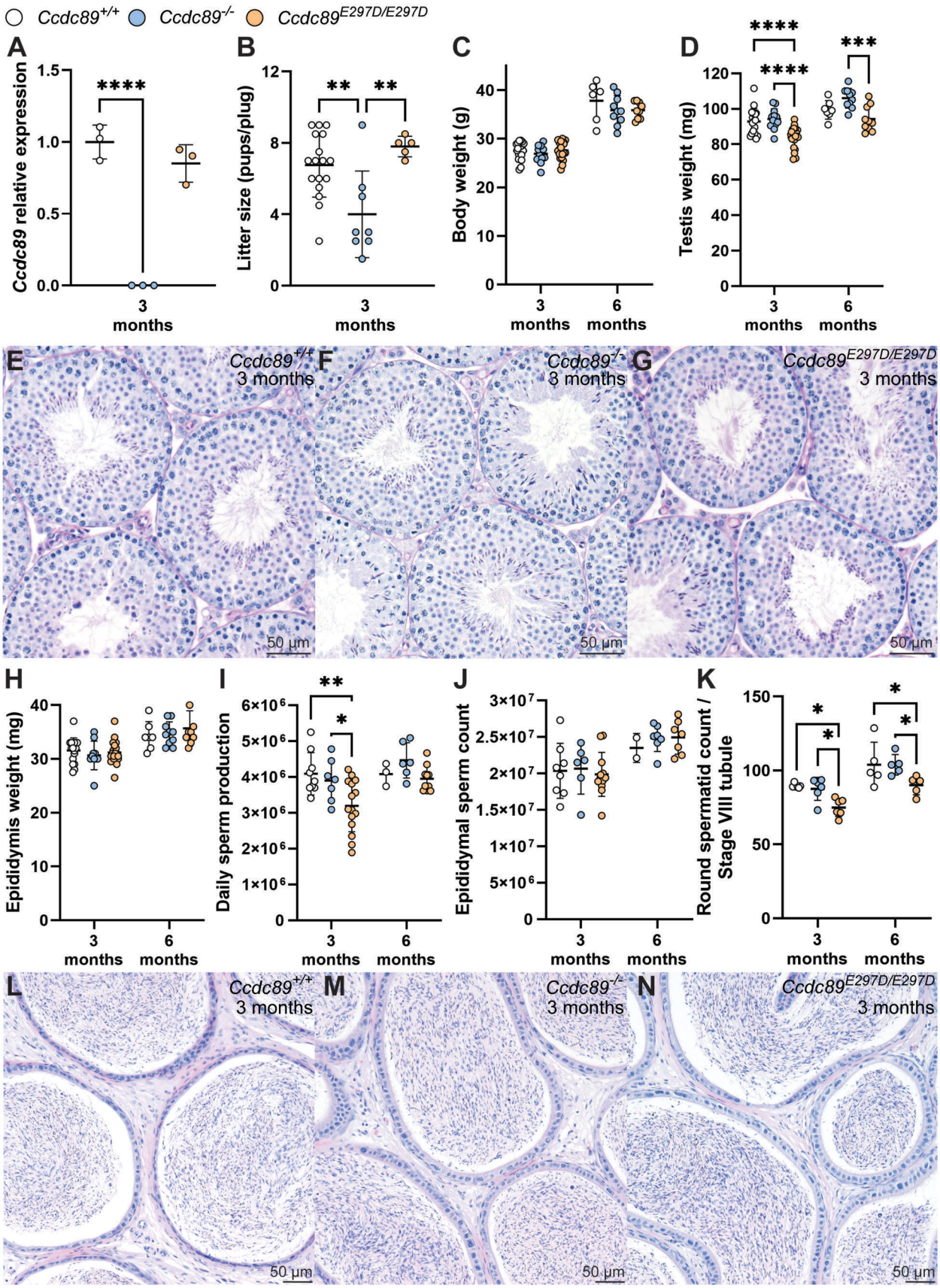

Figure 2. CCDC89 is required for maximal male fertility in mice. Male fertility and *Ccdc89* expression were examined in *Ccdc89*$^{-/-}$ and *Ccdc89*$^{E297D/E297D}$ mutant models compared to wild type, at 3 and 6 months of age. (**A**) *Ccdc89* transcript expression. (**B**) Male fertility assessed as litter size per plug. (**C**) Body weight. (**D**) Testis weight. (**E–G**) Testis histology. (**H**) Epididymis weight. (**I**) Daily sperm production (testis). (**J**) Epididymal sperm count. (**K**) Round spermatid counts in Stage VIII tubules. (**L–N**) Epididymal histology. ****$P < 0.0001$; ***$P < 0.001$; **$P < 0.01$; *$P < 0.05$.

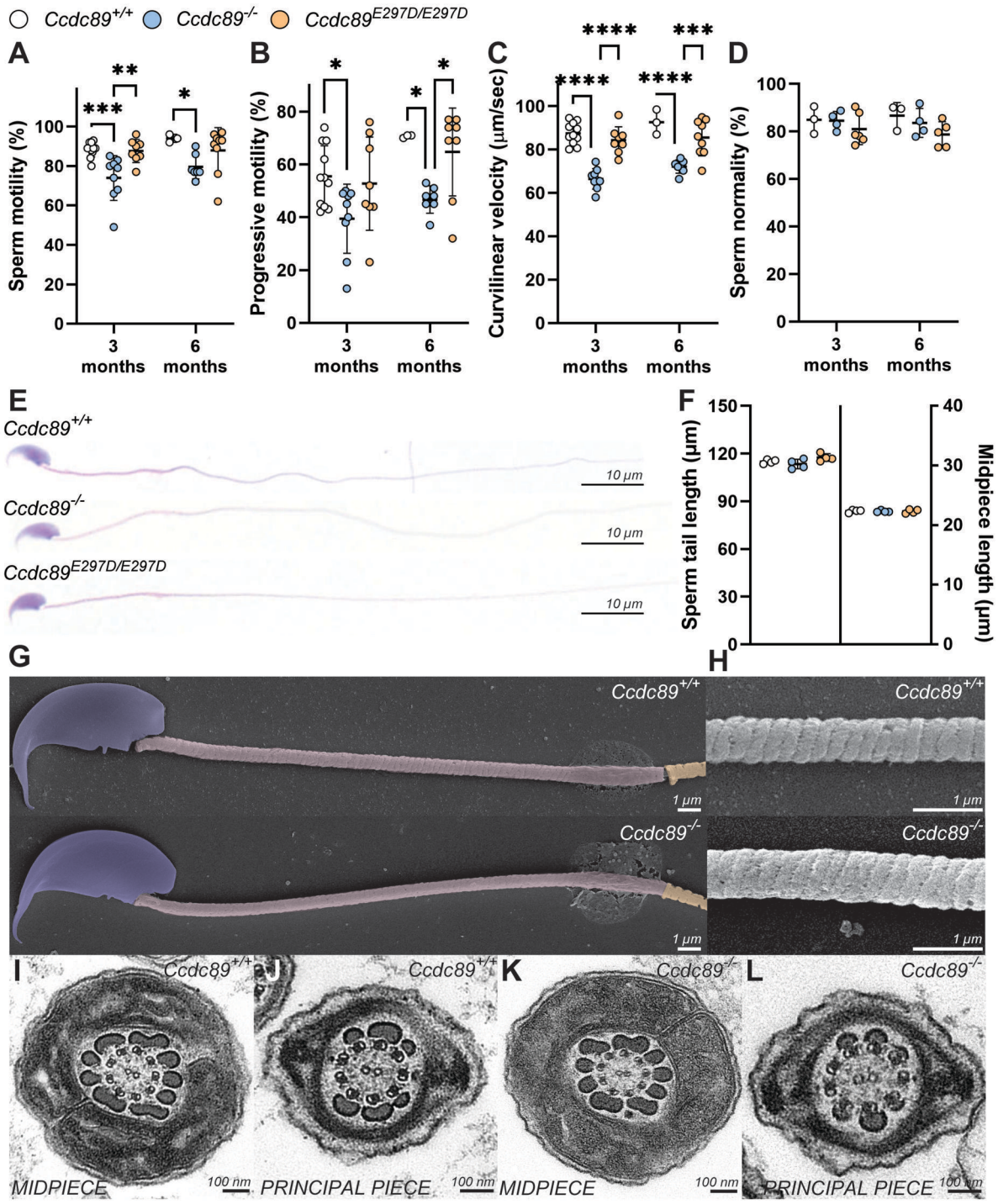

Figure 3. CCDC89 is a regulator of sperm motility in mice. Sperm motility, morphology, and structure were examined in cauda epididymal sperm from *Ccdc89*$^{-/-}$ and *Ccdc89*$^{E297D/E297D}$ mutant models compared to wild type. (**A**) Sperm total motility. (**B**) Progressive sperm motility. (**C**) Curvilinear velocity. (**D**) Sperm morphology normality. (**E**) Sperm cytology. (**F**) Sperm whole tail and midpiece length. (**G, H**) Sperm internal structure assessment on membrane-stripped sperm (scanning electron microscopy), focusing on the mitochondrial sheath (pink in G and uncoloured in H). (**I–L**) Sperm internal structure assessment (transmission electron microscopy) at the midpiece and principal piece level. ****$P < 0.0001$; ***$P < 0.001$; **$P < 0.01$; *$P < 0.05$.

shape cycle was largely overlapping but irregular in shape. Moreover, in mutant sperm with rigid midpieces (Fig. 4Bviii), the shape cycle was poorly overlapping, indicating considerable waveform variability over time. This abnormality in waveform was equally visible by curvature assessment. In wild-type sperm, a largely uniform curvature profile was observed, except in the 10% that exhibited a rigid midpiece (Fig. 4Ci–iv). In contrast, most sperm from *Ccdc89*$^{-/-}$ males (Fig. 4Cvi and vii, stiff and rigid) were asymmetric in their beat cycle. Specifically, the curvature of these sperm altered much more rapidly over each beat cycle, indicating that the waveform failed to propagate effectively along the flagellum. This is demonstrated by the rapid change in red to blue (or blue to red) colouring at each point in time (y-axis). Collectively, these results highlighted a disturbed flagellar wave

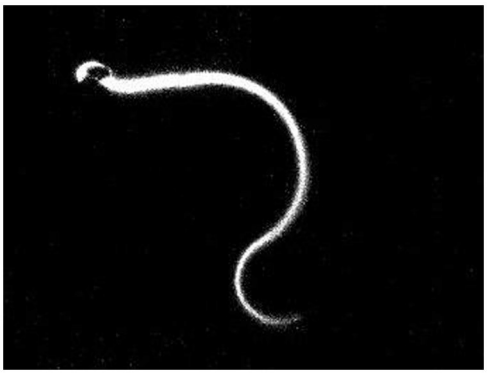

Video 1. Sperm from *Ccdc89*$^{+/+}$ male mice.

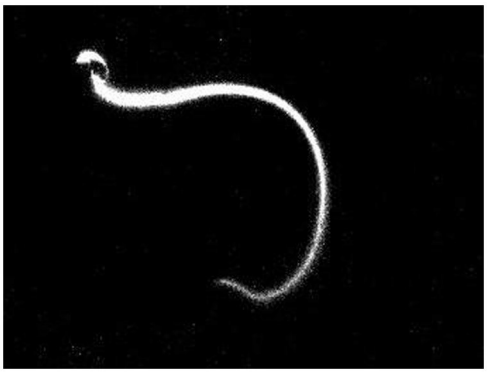

Video 2. Sperm from *Ccdc89*$^{-/-}$ male mice.

with intermitted changes in beating frequency in most sperm from *Ccdc89*$^{-/-}$ males, indicated by sudden gaps in curvature lines. The latter is further reinforced by the presence of two beat frequency peaks in sperm with rigid midpieces (data not shown).

While the average flagella beat frequency was unchanged between genotype (Fig. 5A), a significant 56% reduction in motor input was measured in sperm from *Ccdc89*$^{-/-}$ males (Fig. 5B). This was attributed largely due to the constrained midpiece flexibility (Fig. 5C), as represented in the first 20 microns of the *x*-axis (waveform). Impaired sperm tail flexibility was further evidenced by a 62% reduction in midpiece amplitude (Fig. 5D, $P = 0.004$) as well as a 44% reduction in principal piece amplitude (Fig. 5E, $P = 0.006$) in sperm from *Ccdc89*$^{-/-}$ males compared with wild type. These abnormalities in motility led to significant reductions in energy dissipation from the sperm tail (motor—Fig. 5F, $P = 0.0008$ and internal—Fig. 5G, $P = 0.01$), including total tail hydrodynamic dissipation (Fig. 5H, $P = 0.002$) and hydrodynamic dissipation within the midpiece (Fig. 5I, $P = 0.0001$) and principal piece (Fig. 5J, $P = 0.005$). This energy dissipation directly contributes to the amount of energy delivered to the fluid to propel the sperm.

CCDC89 is required for optimal sperm fertilization *in vitro*

To investigate whether a loss of CCDC89 affected sperm function beyond their ability to traverse the female reproductive tract, we tested the capacity of sperm to fertilize *in vitro* (Fig. 6). While sperm from *Ccdc89*$^{-/-}$ males were capable of achieving fertilization *in vitro*, a 19% reduction in fertilization success was observed compared with wild type (Fig. 6, $P = 0.01$). Consistent with reduced sperm tail flexibility, velocity, and hydrodynamic dissipation, sperm from *Ccdc89*$^{-/-}$ male mice were less capable of penetrating the zona pellucida than sperm from wild-type male mice (not shown).

Discussion

Male fertility relies upon the continuous production of highly motile haploid germ cells. This is achieved via the sequential actions of spermatogonia undergoing mitosis, spermatocytes undergoing meiosis, and the transformation of haploid round spermatids into highly polarized sperm containing structural specializations in their flagellum to support motility within the complex environment of the female reproductive tract. In this study, we present novel genetic and functional data supporting the roles of coiled-coiled domain-containing protein 89 in spermatogenesis and male fertility in both humans and mice. We show that CCDC89 is linked to spermatogenic defects in humans and is required for optimal male fertility in mice, where its molecular function is in the establishment of an effective sperm tail waveform. Specifically, sperm from *Ccdc89*$^{-/-}$ male mice had impaired sperm tail waveform as a consequence of poor midpiece flexibility. Mutant sperm swam more slowly and generated less propulsive power, which would be predicted to impair *in vivo* sperm migration through the female reproductive tract (Yazdan Parast *et al.*, 2023). This loss of functional competence was mirrored in the reduced ability of mutant sperm to achieve fertility *in vitro*, wherein many of the *in vivo* challenges had been removed. While such compromise may not be an absolute determinant of fertility in a monandrous species such as humans, in polyandrous species wherein sperm from multiple males compete for fertilization, such a compromise would be predicted to lead to reduced gene transmission into future generations. That is, males containing a functional CCDC89 gene would be evolutionarily favoured. The perturbed waveform coincided with a significantly reduced sperm tail motor input. Several factors might contribute to this altered waveform, including a reduction in motor input or the consequence of an undetected ultrastructural defect. Nevertheless, these abnormalities in motility resulted in male subfertility and a reduced ability to penetrate the zona pellucida during *in vitro* fertilization experiments.

Here, we detail two unique genetic variants in *CCDC89* identified in three men with non-obstructive azoospermia, providing significant genetic evidence that *CCDC89* is essential for human male fertility. In a biopsy taken from one patient, we observed a Sertoli cell-only presentation, highlighting a potential role of CCDC89 in male germ cell proliferation or viability. In the *Ccdc89*$^{-/-}$ mice generated in this study, however, spermatogenesis was complete, and no differences were seen in germ cell content. This may suggest gene–environment interactions in the men with *CCDC89* variants. Continued genetic studies will inform whether there is a greater dependency on *CCDC89* in humans compared with mice. Although unlikely, patients 1 and 2 who carried a homozygous c. G903T variant may also harbour damaging variants in other genes that exacerbated their fertility presentation. While the precise role of CCDC89 in human spermatogenesis requires more research, the data reported here suggest loss of *CCDC89* function is a risk factor for male infertility. It also underscores the importance of validation studies.

Numerous coiled-coil proteins have been shown to play a role in spermatogenesis (Pasek *et al.*, 2016; Zhang *et al.*, 2022). For example, CCDC proteins have been evidenced to play roles in acrosome and flagellum biogenesis, and in fortifying the sperm head-tail coupling apparatus, such that their loss results in

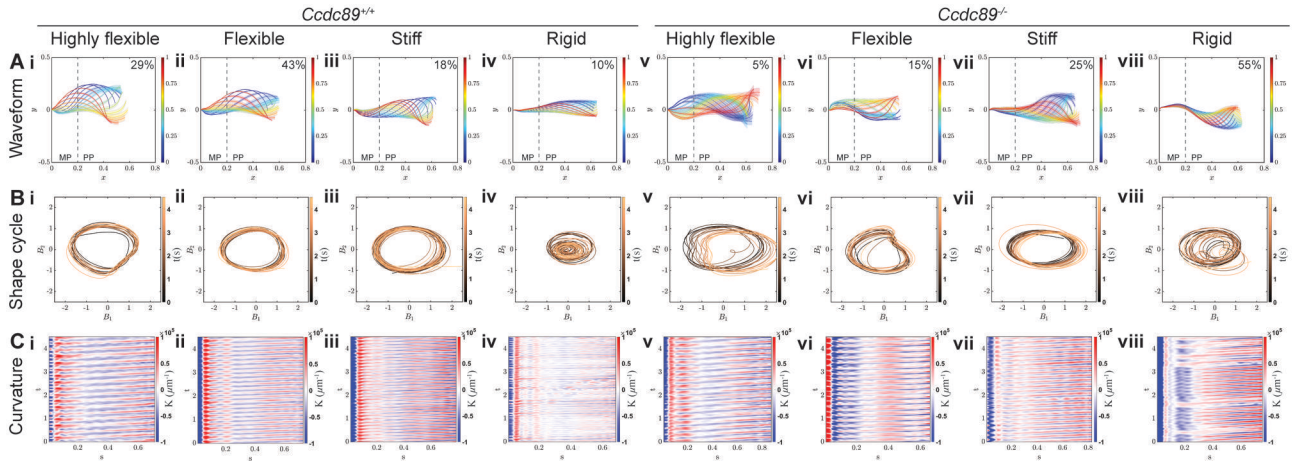

Figure 4. CCDC89 is required for sperm midpiece flexibility and waveform. (**A**) Representative graphs of sperm flagellar waveform from *Ccdc89*$^{+/+}$ and *Ccdc89*$^{-/-}$ males. The four representative categories for midpiece flexibility are shown (highly flexible, flexible, stiff, and rigid). Numbers in the right-hand corner denote the percentage of sperm in each category. (**B**) Shape cycle analysis, where more circular shapes are symmetrical and overlapping circles indicate a repetitive waveform. (**C**) Sperm tail curvature, a depiction of the sperm tail position relative to the midline of the head over multiple cycles. Red represents a position below the sperm head and blue represents a position above the sperm head.

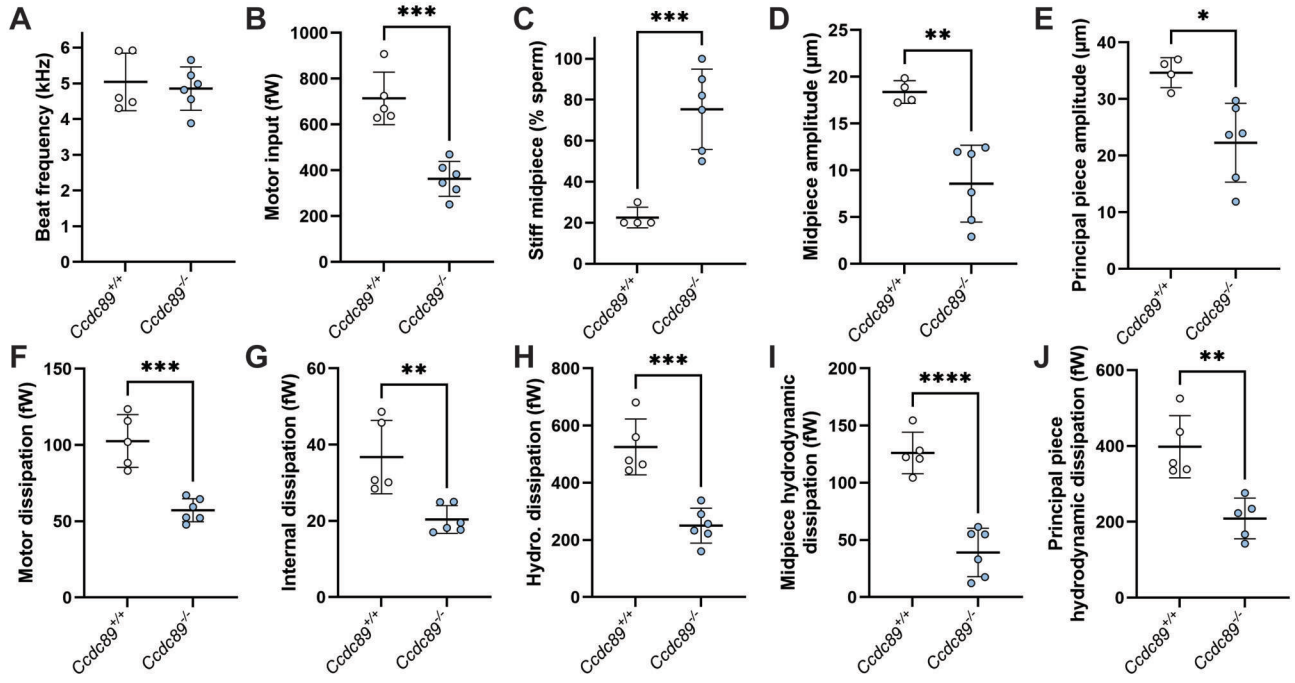

Figure 5. CCDC89 is required for optimal sperm tail flexibility and power utilization. (**A**) Beat frequency. (**B**) Motor input. (**C**) Sperm tail midpiece stiffness assessment. (**D**) Midpiece amplitude. (**E**) Principal piece amplitude. (**F**) Motor dissipation. (**G**) Internal dissipation. (**H–J**) Hydrodynamic dissipation, including specifically within the midpiece and principal piece, respectively. ****$P < 0.0001$; ***$P < 0.001$; **$P < 0.01$. Assessed at 3 months of age.

severe sperm morphological defects (Pasek *et al.*, 2016; Wang *et al.*, 2018, 2023; Zhang *et al.*, 2022). Other CCDC proteins play discrete roles in the regulation of flagella or cilia beating. Two family members, CCDC96 and CCDC113, form a complex in the axoneme that regulates ciliary beating and waveform via roles in connecting radial spoke 3 of the axoneme with the nexin–dynein regulatory complex (Bazan *et al.*, 2021). Loss of either CCDC96 or CCDC113 impairs cilia beat frequency, amplitude, and waveform (Bazan *et al.*, 2021). While the precise role of CCDC89 in male fertility is unclear, we did not detect any significant sperm structural or morphological defects in male mice.

Interestingly, we did identify a reduction in daily sperm production, testis weight, and round sperm numbers in our *Ccdc89*$^{E297D/E297D}$ model. We did not observe any sperm motility defects in the *Ccdc89*$^{E297D/E297D}$ model, suggesting that in this model, CCDC89 may have undergone a partial loss of function in the absence of genetic compensation. When protein function is still partially or fully affected by missense variants, but mRNA is not degraded, then genetic compensation is not triggered (El-Brolosy *et al.*, 2019; Sztal and Stainier, 2020). By comparison in knockout models where premature stop codons are introduced or coding regions are deleted, genetic compensation may occur. This then allows similarly functioning proteins or alternate gene transcripts to be upregulated to compensate. We note that *Ccdc89* only has one coding transcript, but other similarly related genes could be upregulated in the knockout model. As defined by

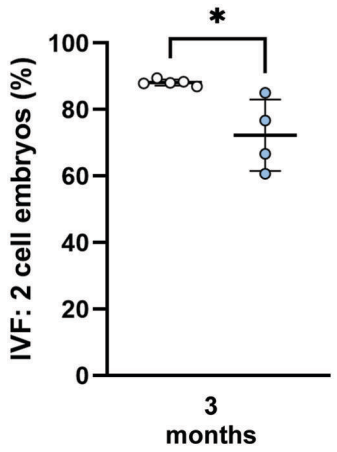

Figure 6. CCDC89 is required for optimal *in vitro* fertilization success. *In vitro* fertilization as assessed by 2-cell formation (n = 20–43 oocytes/replicate, 4–5 animals/genotypes). *$P < 0.05$. Assessed at 3 months of age.

the 3D protein analyses, the introduction of the E297D variant was predicted to only subtly affect protein structure, which may result in the mutant CCDC89 protein mildly affecting germ cell divisions while not affecting the role of CCDC89 in sperm motility. Indeed, due to their versatile protein folding motifs, CCDC proteins play diverse biological roles, including in cell signalling (Burkhard *et al.*, 2001; Starokadomskyy *et al.*, 2013; Azad *et al.*, 2014). Therefore, the difference in the severity of germ cell loss in *Ccdc89*$^{E297D/E297D}$ males compared with that in men with *CCDC89* variants could also be explained by the absence of environmental or lifestyle pressures in mice. Finally, other CCDC proteins could have redundant functions in mice, whereas this may not be the case in humans.

We note that the lack of human sperm in our infertile patients precluded the testing of the contribution of *CCDC89* to human sperm function. Additional sequencing of infertile men, including targeted sequencing for *CCDC89* or a focus on *CCDC89* variants identified by whole exome/genome sequencing, may reveal variants in men with sperm motility defects, which will be important to provide additional evidence for a role of CCDC89 in the regulation of sperm motility in men. These findings will confirm whether CCDC89 function is conserved between mammals.

Collectively, we highlight CCDC89 as a novel regulator of sperm motility in mice that is required for optimal sperm motility. In mice, we identified a role of CCDC89 in establishing sperm midpiece flexibility that in turn affects reproductive success both *in vitro* and *in vivo*. We also identified an effect of replicating the mouse equivalent (p.E297D) of the human p. E301D genetic variant on germ cell content, which may be relevant to the infertility phenotype in the three azoospermic men affected by this variant.

Supplementary data

Supplementary data are available at *Human Reproduction* online.

Data availability

Data are available upon request to the corresponding author.

Authors' roles

M.K.O.B., K.A., and B.J.H. designed the experiments. G.S., J.N., S.B.W., A.E.O.C., M.G., J.E.M.D., and B.J.H. undertook the experiments. M.K.O.B., G.S., S.B.W., D.F.C., R.N., K.A., and B.J.H. analysed the data. M.K.O.B. and B.J.H. wrote the paper. The patients' DNA was sequenced and validated by D.F.C. and H.C.-M. All authors provided intellectual input and feedback on drafts. All authors reviewed and approved the final publication.

Funding

This work was supported by a National Health and Medical Research Council grant awarded to M.K.O.B. and D.F.C. (APP1120356), National Institutes of Health grants to D.F.C. (R01HD078641 and P50HD096723), the Novo Nordisk Foundation (grant numbers NNF210C0069913 and NNF21C0069969), the Capital Region of Denmark, the Independent Research Fund (grant number 1030-00381B), and the Svend Andersen Foundation (grant number 84-A.08) awarded to K.A., and the Christian and Ottilia Brorsons (No. 12038-1) and Frimodt-Heineke Foundation Travel Grants for research exchange awarded to G.S.

Conflict of interest

None declared.

References

Azad AK, Chakrabarti S, Xu Z, Davidge ST, Fu Y. Coiled-coil domain containing 3 (CCDC3) represses tumor necrosis factor-alpha/nuclear factor kappaB-induced endothelial inflammation. *Cell Signal* 2014;**26**:2793–2800.

Bazan R, Schrofel A, Joachimiak E, Poprzeczko M, Pigino G, Wloga D. Ccdc113/Ccdc96 complex, a novel regulator of ciliary beating that connects radial spoke 3 to dynein g and the nexin link. *PLoS Genet* 2021;**17**:e1009388.

Burkhard P, Stetefeld J, Strelkov SV. Coiled coils: a highly versatile protein folding motif. *Trends Cell Biol* 2001;**11**:82–88.

Djureinovic D, Fagerberg L, Hallstrom B, Danielsson A, Lindskog C, Uhlen M, Ponten F. The human testis-specific proteome defined by transcriptomics and antibody-based profiling. *Mol Hum Reprod* 2014;**20**:476–488.

Dunleavy JEM, Graffeo M, Wozniak K, O'Connor AE, Merriner DJ, Nguyen J, Schittenhelm RB, Houston BJ, O'Bryan MK. The katanin A-subunits KATNA1 and KATNAL1 act co-operatively in mammalian meiosis and spermiogenesis to achieve male fertility. *Development* 2023;**150**:dev201956.

Dunleavy JEM, O'Connor AE, Okuda H, Merriner DJ, O'Bryan MK. KATNB1 is a master regulator of multiple katanin enzymes in male meiosis and haploid germ cell development. *Development* 2021;**148**:dev199922.

Dunleavy JEM, Okuda H, O'Connor AE, Merriner DJ, O'Donnell L, Jamsai D, Bergmann M, O'Bryan MK. Katanin-like 2 (KATNAL2) functions in multiple aspects of haploid male germ cell development in the mouse. *PLoS Genet* 2017;**13**:e1007078.

El-Brolosy MA, Kontarakis Z, Rossi A, Kuenne C, Gunther S, Fukuda N, Kikhi K, Boezio GLM, Takacs CM, Lai SL *et al.* Genetic compensation triggered by mutant mRNA degradation. *Nature* 2019;**568**:193–197.

Fagerberg L, Hallstrom BM, Oksvold P, Kampf C, Djureinovic D, Odeberg J, Habuka M, Tahmasebpoor S, Danielsson A, Edlund K *et al.* Analysis of the human tissue-specific expression by genome-wide integration of transcriptomics and antibody-based proteomics. *Mol Cell Proteomics* 2014;**13**:397–406.

Gaikwad AS, Nandagiri A, Potter DL, Nosrati R, O'Connor AE, Jadhav S, Soria J, Prabhakar R, O'Bryan MK. CRISPs function to boost

sperm power output and motility. *Front Cell Dev Biol* 2021; **9**:693258.

Houston BJ, Conrad DF, O'Bryan MK. A framework for high-resolution phenotyping of candidate male infertility mutants: from human to mouse. *Hum Genet* 2021a;**140**:155–182.

Houston BJ, Merriner DJ, Stathatos GG, Nguyen JH, O'Connor AE, Lopes AM, Conrad DF, Baker M, Dunleavy JE, O'Bryan MK. Genetic mutation of Cep76 results in male infertility due to abnormal sperm tail composition. *Life Sci Alliance* 2024; **7**:e202302452.

Houston BJ, Nagirnaja L, Merriner DJ, O'Connor AE, Okuda H, Omurtag K, Smith C, Aston KI, Conrad DF, O'Bryan MK. The Sertoli cell expressed gene secernin-1 (Scrn1) is dispensable for male fertility in the mouse. *Dev Dyn* 2021b;**250**:922–931.

Houston BJ, O'Connor AE, Wang D, Goodchild G, Merriner DJ, Luan H, Conrad DF, Nagirnaja L, Aston KI, Kliesch S *et al.* Human INHBB gene variant (c.1079T>C: p.Met360Thr) alters testis germ cell content, but does not impact fertility in mice. *Endocrinology* 2022;**163**:bqab269.

Houston BJ, Riera-Escamilla A, Wyrwoll MJ, Salas-Huetos A, Xavier MJ, Nagirnaja L, Friedrich C, Conrad DF, Aston KI, Krausz C *et al.* A systematic review of the validated monogenic causes of human male infertility: 2020 update and a discussion of emerging gene-disease relationships. *Hum Reprod Update* 2021c;**28**:15–29.

Hu J, Merriner DJ, O'Connor AE, Houston BJ, Furic L, Hedger MP, O'Bryan MK. Epididymal cysteine-rich secretory proteins are required for epididymal sperm maturation and optimal sperm function. *Mol Hum Reprod* 2018;**24**:111–122.

Jumper J, Evans R, Pritzel A, Green T, Figurnov M, Ronneberger O, Tunyasuvunakool K, Bates R, Zidek A, Potapenko A *et al.* Highly accurate protein structure prediction with AlphaFold. *Nature* 2021;**596**:583–589.

Jung M, Wells D, Rusch J, Ahmad S, Marchini J, Myers SR, Conrad DF. Unified single-cell analysis of testis gene regulation and pathology in five mouse strains. *Elife* 2019;**8**:e43966.

Kircher M, Witten DM, Jain P, O'Roak BJ, Cooper GM, Shendure J. A general framework for estimating the relative pathogenicity of human genetic variants. *Nat Genet* 2014;**46**:310–315.

Korneev D, Merriner DJ, Gervinskas G, de Marco A, O'Bryan MK. New insights into sperm ultrastructure through enhanced scanning electron microscopy. *Front Cell Dev Biol* 2021;**9**:672592.

Krausz C, Riera-Escamilla A. Genetics of male infertility. *Nat Rev Urol* 2018;**15**:369–384.

Li Q, Wang K. InterVar: clinical interpretation of genetic variants by the 2015 ACMG-AMP guidelines. *Am J Hum Genet* 2017; **100**:267–280.

Lord T, Nixon B, Jones KT, Aitken RJ. Melatonin prevents postovulatory oocyte aging in the mouse and extends the window for optimal fertilization in vitro. *Biol Reprod* 2013;**88**:67.

Martin JH, Aitken RJ, Bromfield EG, Cafe SL, Sutherland JM, Frost ER, Nixon B, Lord T. Investigation into the presence and functional significance of proinsulin C-peptide in the female germlinedagger. *Biol Reprod* 2019;**100**:1275–1289.

Mirdita M, Schutze K, Moriwaki Y, Heo L, Ovchinnikov S, Steinegger M. ColabFold: making protein folding accessible to all. *Nat Methods* 2022;**19**:679–682.

Moutevelis E, Woolfson DN. A periodic table of coiled-coil protein structures. *J Mol Biol* 2009;**385**:726–732.

Nagirnaja L, Lopes AM, Charng WL, Miller B, Stakaitis R, Golubickaite I, Stendahl A, Luan T, Friedrich C, Mahyari E *et al.* Diverse monogenic subforms of human spermatogenic failure. *Nat Commun* 2022;**13**:7953.

Nandagiri A, Gaikwad AS, Potter DL, Nosrati R, Soria J, O'Bryan MK, Jadhav S, Prabhakar R. Flagellar energetics from high-resolution imaging of beating patterns in tethered mouse sperm. *Elife* 2021; **10**:e62524.

Nielsen JE, Rolland AD, Rajpert-De Meyts E, Janfelt C, Jorgensen A, Winge SB, Kristensen DM, Juul A, Chalmel F, Jegou B *et al.* Characterisation and localisation of the endocannabinoid system components in the adult human testis. *Sci Rep* 2019;**9**:12866.

Pasek RC, Malarkey E, Berbari NF, Sharma N, Kesterson RA, Tres LL, Kierszenbaum AL, Yoder BK. Coiled-coil domain containing 42 (Ccdc42) is necessary for proper sperm development and male fertility in the mouse. *Dev Biol* 2016;**412**:208–218.

Pir MS, Begar E, Yenisert F, Demirci HC, Korkmaz ME, Karaman A, Tsiropoulou S, Firat-Karalar EN, Blacque OE, Oner SS *et al.* CilioGenics: an integrated method and database for predicting novel ciliary genes. *Nucleic Acids Res* 2024;**52**:8127–8145.

Powar S, Parast FY, Nandagiri A, Gaikwad AS, Potter DL, O'Bryan MK, Prabhakar R, Soria J, Nosrati R. Unraveling the kinematics of sperm motion by reconstructing the flagellar wave motion in 3D. *Small Methods* 2022;**6**:e2101089.

Priyanka PP, Yenugu S. Coiled-coil domain-containing (CCDC) proteins: functional roles in general and male reproductive physiology. *Reprod Sci* 2021;**28**:2725–2734.

Robinson JT, Thorvaldsdottir H, Winckler W, Guttman M, Lander ES, Getz G, Mesirov JP. Integrative genomics viewer. *Nat Biotechnol* 2011;**29**:24–26.

Salehi N, Karimi-Jafari MH, Totonchi M, Amiri-Yekta A. Integration and gene co-expression network analysis of scRNA-seq transcriptomes reveal heterogeneity and key functional genes in human spermatogenesis. *Sci Rep* 2021;**11**:19089.

Starokadomskyy P, Gluck N, Li H, Chen B, Wallis M, Maine GN, Mao X, Zaidi IW, Hein MY, McDonald FJ *et al.* CCDC22 deficiency in humans blunts activation of proinflammatory NF-kappaB signaling. *J Clin Invest* 2013;**123**:2244–2256.

Sztal TE, Stainier DYR. Transcriptional adaptation: a mechanism underlying genetic robustness. *Development* 2020;**147**:dev186452.

Tapia Contreras C, Hoyer-Fender S. CCDC42 localizes to Manchette, HTCA and tail and interacts with ODF1 and ODF2 in the formation of the male germ cell cytoskeleton. *Front Cell Dev Biol* 2019; **7**:151.

Utterstrom J, Naeimipour S, Selegard R, Aili D. Coiled coil-based therapeutics and drug delivery systems. *Adv Drug Deliv Rev* 2021; **170**:26–43.

Varadi M, Bertoni D, Magana P, Paramval U, Pidruchna I, Radhakrishnan M, Tsenkov M, Nair S, Mirdita M, Yeo J *et al.* AlphaFold Protein Structure Database in 2024: providing structure coverage for over 214 million protein sequences. *Nucleic Acids Res* 2024;**52**:D368–D375.

Wang M, Kang J, Shen Z, Hu Y, Chen M, Cui X, Liu H, Gao F. CCDC189 affects sperm flagellum formation by interacting with CABCOCO1. *Natl Sci Rev* 2023;**10**:nwad181.

Wang T, Yin Q, Ma X, Tong MH, Zhou Y. Ccdc87 is critical for sperm function and male fertility. *Biol Reprod* 2018;**99**:817–827.

Wiel L, Baakman C, Gilissen D, Veltman JA, Vriend G, Gilissen C. MetaDome: pathogenicity analysis of genetic variants through aggregation of homologous human protein domains. *Hum Mutat* 2019;**40**:1030–1038.

Wiel L, Venselaar H, Veltman JA, Vriend G, Gilissen C. Aggregation of population-based genetic variation over protein domain homologues and its potential use in genetic diagnostics. *Hum Mutat* 2017;**38**:1454–1463.

Yang Y, Cochran DA, Gargano MD, King I, Samhat NK, Burger BP, Sabourin KR, Hou Y, Awata J, Parry DA *et al.* Regulation of flagellar motility by the conserved flagellar protein CG34110/Ccdc135/FAP50. *Mol Biol Cell* 2011;**22**:976–987.

Yazdan Parast F, Gaikwad AS, Prabhakar R, O'Bryan MK, Nosrati R. The cooperative impact of flow and viscosity on sperm flagellar energetics in biomimetic environments. *Cell Rep Phys Sci* 2023; **4**:101646.

Zhang R, Wu B, Liu C, Zhang Z, Wang X, Wang L, Xiao S, Chen Y, Wei H, Jiang H *et al.* CCDC38 is required for sperm flagellum biogenesis and male fertility in mice. *Development* 2022; **149**:dev200516.

Human Reproduction, 2025, 40, 1616–1628
https://doi.org/10.1093/humrep/deaf126
Original Article